Atomic Photo-Ionization Cross Sections from a Semiempirical Central Potential*†

EUGENE J. MCGUIRE‡

Laboratory of Atomic and Solid-State Physics and Department of Physics, Cornell University, Ithaca, New York

(Received 2 August 1966; revised manuscript received 27 April 1967)

The exact solutions for the Schrödinger equation with a central potential of the form $V(r)=2Z/r-\Delta$, $r\leq r_1$; $V(r)=2/r$, $r\geq r_1$; $r_1=2(Z-1)/\Delta$ are developed. Z and Δ are chosen to fit observed term values for various atoms, and the parametrized continuum orbitals are used to calculate the photo ionization cross section of these atoms. For certain transitions the photo-ionization cross-section matrix element can be written as an exact expression. This is done for valence photo-ionization in He and the alkalis, for $4d$-shell photo-ionization in the elemets indium to xenon, and for the $3d$ shell in krypton. The relationship between this approach and the Coulomb method of Burgess and Seaton is briefly discussed.

I. INTRODUCTION

QUANTUM-MECHANICAL calculations of the atomic photoabsorption process have been of three types. The earliest attempts at systematic study utilized the results obtained for the hydrogen atom.[1] These results for the hydrogen isoelectronic sequence were compared with x-ray atomic absorption coefficients and reasonable agreement was found at sufficiently short wavelengths if a suitable effective charge were inserted in the hydrogenic formulas.[2] When applied to the optical and ultraviolet region these calculations were generally in error, often by orders of magnitude. The Coulomb approximation[3,4] was developed to treat the optical photoabsorption processes. It was argued that in this wavelength region the relevant nondiagonal matrix element in the calculation was determined by the behavior of the active electron orbitals at large distances from the core of the atom. The Schrödinger equation for the hydrogen atom can be solved in terms of the regular and irregular Coulomb wave functions, but the boundary conditions allow only the degenerate solution, where the Wronskian of the regular and irregular solution vanishes. The solutions are then Laguerre polynomials. The Coulomb approximation leads to the Schrödinger equation for the hydrogen atom, but it evades the boundary condition at $r=0$. The large r solutions for bound states are the irregular Coulomb functions while for the continuum both solutions are allowed. The core region is to some extent accounted for by the use of experimental term values and ionization energies in the approximation. Calculations[5] are in reasonable agreement with experiment in the alkalis and for transitions involving two excited states, i.e., at large distances. However, when one deals with photo-ionization of the alkalis in the far ultraviolet or photoabsorption by atoms with complicated valence shells the large distance approximation fails; i.e., the core becomes important.

Finally there have been some recent studies of atomic photo-ionization using the modified Hartree-Fock approaches.[6,7] So far, these have only mixed success in reproducing experimental results. It is doubtful that these calculations, in L-S coupling, require more accurate ground-state wave functions than those provided in the work of Herman and Skillman.[8] If this is so, then the principal error in these calculations will be in the continuum state orbitals, i.e., the normalization, orthogonality, and position of the nodes of the continuum orbital as a function of energy.

In the following, we will develop the exact solution to the Schrödinger equation with a central potential more complicated than that for the hydrogen atom. At large distances, the solutions are the same as those of the Coulomb model, but there is an explicit boundary at which we join inner and outer solutions. The boundary which is determined from experimental term values allows one to satisfy the boundary conditions at both $r=0$ and $r=\infty$. The continuum orbitals are then used to compute photo-ionization cross sections in the optical and soft x-ray regions.

II. THE MODEL

The one-electron radial Schrödinger equation is

$$[d^2/dr^2+V(r)-l(l+1)/r^2+E]\phi(r)=0. \quad (1)$$

For the hydrogen atom $V(r)=2/r$ (in Rydberg units) and the boundary conditions are $\phi(0)=0$, $\phi(\infty)$

---

* Based on a thesis submitted in partial fulfillment of the requirements for the degree of Doctor of Philosophy.

† Supported in part by U.S. Army Research Office (Durham) and in part by the U.S. Atomic Energy Commission.

‡ Now at Sandia Corporation, Albuquerque, New Mexico.

[1] M. Stobbe, Ann. Physik **7**, 661 (1930).

[2] H. Hall, Rev. Mod. Phys. **8**, 358 (1936).

[3] M. J. Seaton, Monthy Notices Roy. Astron. Soc. **118**, 504 (1958); A. Burgess and M. J. Seaton, *ibid.* **120**, 121 (1960).

[4] D. R. Bates and A. Damgaard, Phil. Trans. Roy. Soc. (London) **A242**, 101 (1949).

[5] J. E. Solarski and W. L. Wiese, Phys. Rev. **135**, A1236 (1964).

[6] J. W. Cooper, Phys. Rev. **128**, 681 (1962).

[7] K. G. Sewell, Phys. Rev. **138**, A418 (1965).

[8] F. Herman and S. Skillman, *Atomic Structure Calculations* (Prentice-Hall, Inc., Englewood Cliffs, New Jersey, 1963).

bounded. The Coulomb approximation for atoms is $V(r)=2/r$ with the boundary condition $\phi(\infty)$ bounded. Since, in the Coulomb approximation, the behavior of the orbital at small distances is neglected, a factor $f(r)$ is introduced such that $f(r)\phi(r)$ goes to zero when r goes to zero and $f(r)=1$ for the region where the Coulomb approximation is valid. However, $f(r)\phi(r)$ does not satisfy the Schrödinger equation and the validity of the Coulomb approximation is questionable when $f(r)$ enters the calculation. We avoid the difficulty with the small r behavior by using a potential

$$V(r)=2Z/r-\Delta, \qquad r\leq r_1$$
$$V(r)=2/r, \qquad r\geq r_1$$

and

$$r_1=2(Z-1)/\Delta. \tag{2}$$

Here Z is chosen to approximate the outer portion of the atomic charge density and Δ is chosen to fit the discrete level energies of the model to those observed for the system.

Using

$$\nu=1/(-E)^{1/2}, \qquad E\leq 0$$
$$K=1/E^{1/2}, \qquad E\geq 0$$
$$\alpha=Z/(\Delta-E)^{1/2}, \qquad E<\Delta \tag{3a}$$

the solutions to the Schrödinger equation are

$$\phi_1(r)=AM_{\alpha,l+1/2}(2rZ/\alpha), \qquad r\leq r_1$$
$$\phi_2(r)=BW_{\nu,l+1/2}(2r/\nu), \qquad r\geq r_1 \quad \text{for} \quad E\leq 0 \tag{3b}$$

and

$$\phi_1(r)=AM_{\alpha,l+1/2}(2rZ/\alpha), \qquad r\leq r_1$$
$$\phi_2(r)=B[M_{iK,l+1/2}(2r/iK)+CW_{iK,l+1/2}(2r/iK)], \qquad r\geq r_1 \quad \text{for} \quad E\geq 0. \tag{3c}$$

A, B, and C are constants; A and B are found from the normalization and C from the eigenvalue equation. $M_{k,m}(X)$ and $W_{k,m}(X)$ are Whittaker[9] functions and are discussed briefly in Appendix A. The solutions (3b) and (3c) satisfy both the Schrödinger equation and the boundary conditions. In addition, we impose the conditions that ϕ and $d\phi/dr$ be continuous at $r=r_1$, and we normalize the continuum orbital to[10]

$$\phi_2(\text{large } r)\approx(K/\pi)^{1/2} \times \cos[r/K+K\ln(2r/K)-\pi(l+1)/2+\sigma_l].$$

This agrees with the normalization in Ref. 3 up to a factor $(\pi)^{1/2}$.

Before we explicitly satisfy these conditions, we follow Hartree[11] in decomposing the Whittaker function:

$$M_{\nu,l+1/2}(2r/\nu)=(2l+1)!\,G_l(r,1/\nu^2)/(\nu)^{l+1},$$
$$(-\nu)^{l+1}W_{\nu,l+1/2}(2r/\nu)/\Gamma(l+1+\nu)=G_l(r,1/\nu^2) \times\cos\pi\nu+H_l(r,1/\nu^2)\sin\pi\nu \quad \text{for} \quad E<0(\nu \text{ real}). \tag{4a}$$

For $E>0(\nu\to iK)$ we have

$$M_{iK,l+1/2}(2r/iK)=(2l+1)!\,G_l(r,-1/K^2)/(-iK)^{l+1}, \tag{4b}$$
$$(-iK)^{l+1}W_{iK,l+1/2}(2r/iK)/\Gamma(l+1+iK) =e^{\pi K}G_l(r,-1/K^2)/2+i\sinh(\pi K)H_l'(r,-1/K^2). \tag{4c}$$

Here G_l, H_l, and H_l' are real functions of E.

$H_l(r,1/\nu^2)$ differs from $H_l'(r,1/K^2)$ but $H_l(r,0)=H_l'(r,0)$. This difference as well as the reality of these three functions is discussed in the author's thesis.[12] G_l and H_l' are computed from the real and imaginary parts of the left-hand side of Eq. (4c). G_l determined from Eq. (4b) differed from G_l of Eq. (4c) by less than one part in one hundred for the range of parameters checked.

With these functions the continuity conditions for $E<0$ lead to the eigenvalue equation

$$\tan\pi\nu=-[M_{\alpha,l+1/2}(2rZ/\alpha),G_l(r,1/\nu^2)]/[M_\alpha,H_l], \tag{5a}$$

where

$$[\phi_1(ar),\phi_2(br)]=\left(\phi_1\frac{d\phi_2}{dr}-\phi_2\frac{d\phi_1}{dr}\right)\Bigg|_{r=r_1}. \tag{5b}$$

For ν large $\alpha\to Z/\sqrt{\Delta}$, and

$$\lim_{\nu\to\infty}G_l(r,1/\nu^2)=\sqrt{(2r)}J_{2l+1}(\sqrt{(8r)}),$$
$$\lim_{\nu\to\infty}H_l(r,1/\nu^2)=\sqrt{(2r)}Y_{2l+1}(\sqrt{(8r)}), \tag{6a}$$

and the eigenvalue equation is

$$\tan\pi\nu=\text{constant}. \tag{6b}$$

This leads to a Rydberg series. For ν small, the eigenvalue equation is solved by fixing l, Z, and ν and varying Δ to satisfy (5a). One obtains a series of contours of Δ versus ν, an example of which is shown in Fig. 1 for $Z=9$, $l=1$. The properties of such contours have been investigated,[13] and are summarized in Appendix B.

From the asymptotic expansion[14] for the Whittaker functions and the continuity conditions, the normalized

[9] E. T. Whittaker and G. N. Watson, *Modern Analysis* (Cambridge University Press, London, 1945).
[10] E. Fues, Ann. Physik **87**, 281 (1926).
[11] D. R. Hartree, Proc. Cambridge Phil. Soc. **24**, 426 (1928).
[12] E. J. McGuire, thesis, Cornell University, 1965 (unpublished).
[13] U.S. Army Research Office Technical Report No. 7-ARO(D), 1965 (unpublished).
[14] L. J. Slater, *Confluent Hypergeometric Functions* (Cambridge University Press, London, 1960).

continuum orbital is found to be

$$\phi_1(E,l,r)=M_{\alpha,l+1/2}(2rZ/\alpha)/A_1R, \qquad r\leq r_1$$
$$\phi_2(E,l,r)=A_1[G_l(r,-1/K^2)\cos\theta-H_l'(r,-1/K^2)\times(1-e^{-2\pi K})\sin\theta], \qquad r\geq r_1 \tag{7}$$

where

$$A_1=[\prod_{\lambda=1}^{l}(1+\lambda^2/K^2)/2(1-e^{-2\pi K})]^{1/2},$$
$$\cos\theta=(1-e^{-2\pi K})[M_\alpha, H_l']/R,$$
$$\sin\theta=[M_\alpha, G_l]/R,$$
$$R=\{[M_\alpha, G_l]^2+(1-e^{-2\pi K})^2[M_\alpha, H_l']^2\}^{1/2}.$$

If we use ν_n as the nth solution of the eigenvalue equation and define $\mu_n=n-\nu_n$ as the quantum defect, then it is trivial to show that

$$\lim_{n\to\infty}\pi\mu_n=\lim_{K\to\infty}\theta=\theta^{\text{th}}. \tag{8}$$

Further, if the bound-state orbital is normalized for ν large such that[15]

$$\lim_{r\to\infty}\phi_B(1/\nu^2,l,r)=(2r/\nu)^\nu e^{-r/\nu}[\nu^2\Gamma(\nu-l)\,\Gamma(\nu+l+1)]^{-1/2}, \tag{9a}$$

then

$$\lim_{\nu_n\to\infty}(\tfrac{1}{2}\nu_n^3)^{1/2}\phi_B(1/\nu_n^2,l;r)=\lim_{K\to\infty}\phi_C(1/K^2,l;r). \tag{9b}$$

Here, the subscripts B and C refer to bound and continuum, respectively. The first relation [Eq. (8)] connects the extrapolated quantum defect to the continuum threshold phase shift, and was explicitly used in the quantum-defect method. The second limit relation [Eq. (9b)] assures oscillator density continuity and was implicitly used in Ref. 3.

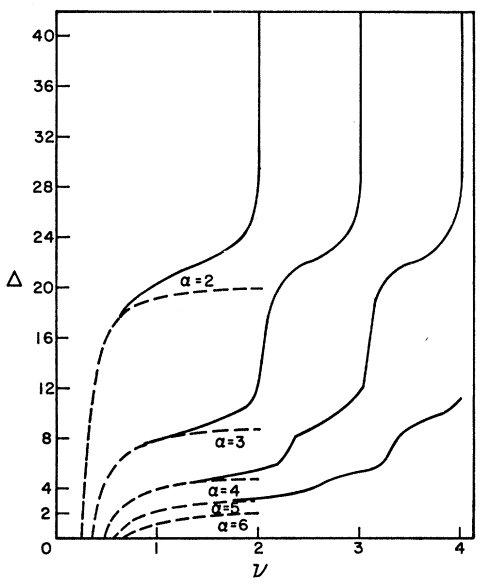

FIG. 1. Loci of allowed solutions to the boundary condition for $Z=9$, $l=1$.

[15] D. R. Hartree, Proc. Cambridge Phil. Soc. **24**, 89 (1928).

In the quantum-defect method Burgess and Seaton[3] develop an orbital for $r\geq r_1$, which is similar to $\phi_2(r)$ of Eq. (7). They use the discrete level data to expand μ_n as a power series in the energy to continue μ_n into the continuum. Because the available spectral data is finite for any atomic system, the continuation of μ_n into the continuum is not unique and their method is limited to regions of the spectrum near threshold. A similar situation confronts us when we attempt to use a spectral plot such as Fig. 1 to find Δ, given some spectral data. There are several values of Δ which can reasonably reproduce the observed spectral data, i.e., the core is not unique. In Sec. IV, we employ some additional information to choose a unique Δ. But when the inner region is irrelevant in a calculation, the quantum-defect orbital should be sufficient.

III. THE PHOTO-IONIZATION CROSS SECTION

In the dipole length approximation the photo-ionization cross section is given by[3]

$$\sigma_\nu=\frac{8\pi^3e^2\nu a_0^2}{3C}\sum_{l'=l\pm1}C_{l'}\left|\int_0^\infty P_i(l:r)rP_f(E,l':r)\,dr\right|^2, \tag{10}$$

where ν is the frequency of the incident photon and $C_{l'}$ is a factor which arises from averaging over initial and summing over final states. In numerical terms,

$$\sigma_\nu=8.56\times\pi\times10^{-19}E\sum C_{l'}\left|\int P_irP_f dr\right|^2$$
$$=8.56\times\pi\times10^{-19}E\sum C_{l'}M_{if}^2, \tag{11}$$

where the cross section is in cm^2 when the energy is in Rydbergs and the orbitals are normalized as we have done in the previous section. This expression formally assumes an unrelaxed core approximation[6] in that the overlap integral for the passive electrons in the initial and final states is set equal to unity. This effect is not entirely neglected in a semiempirical calculation using experimental term values and ionization thresholds; that is, core relaxation is completely included in the energy values used, but completely neglected in the matrix element calculations.

In terms of the model orbitals,

$$M_{if}=\int_0^{r_1}P_i(r)rP^-(E,l';r)\,dr+\int_{r_1}^\infty P_i(r)rP^+(E,l';r)\,dr$$
$$=M_{if}^-+M_{if}^+. \tag{12}$$

Generally a numerical integration is required at this point. However, when r_1 is either so large that M_{if}^+ can be neglected, or so small that M_{if}^- can be neglected,

the integrals can be done in analytical form. The former case covers x-ray transitions and is discussed in Sec. VI. The latter case is treated in the following. It is similar to the treatment of Ref. 3, but explicitly derives the cross-section expression.

For the ground-state orbital, we use a function of the form[4]

$$P_i(r)=A_2 r^{\nu}e^{-r/\nu}(1+b_1/r+b_2/r^2). \quad (13)$$

This is fitted to the available Hartree or Hartree-Fock orbital. The constants b_1 and b_2 are chosen to fit the outer nodes, if any, of the Hartree orbital and the overall function is normalized to fit the large r tail, i.e., A_2. Using this approximate orbital, accurate at large and intermediate distances, introduces a term of the form $(r)^{\nu-2}$ which may diverge at small r. However, in the matrix element evaluation the b_2 term in the expansion is rarely significant. The exponential in the expansion permits the integrals in the matrix element to be done by reference to tables of Laplace transforms.[14] When the inner region can be neglected, we have

$$\int_{r_1}^{\infty}P_i(r)rP^+(E,l;r)\,dr\approx\int_0^{\infty}P_i(r)rP^+(E,l;r)\,dr. \quad (14)$$

Then

$$M_{if}=A_2\sum_{t=0}^{2}b_t\int_0^{\infty}r^{\nu+1-t}e^{-r/\nu}\phi_2(1/K^2,l;r)\,dr, \quad (15)$$

where $\phi_2(1/K^2,l;r)$ is given by Eq. (7). These integrals are finite when $\nu+2-t-l>0$. In all the computations of Sec. V, this condition is satisfied. The use of $\int_0^{r_1}P_irP^+(E,l;r)\,dr$ in place of $\int_0^{r_1}P_irP^-(E,l;r)\,dr$ involves not only the assertion that the latter integral is small, but that the former is small as well. Numerical calculations have verified that both assertions are valid for the limited spectral range covered in Sec. V. The integral is done in Appendix C and the final result is

$$M_{if}=C\sum_t b_t\Gamma(\nu+3+l-t)\Gamma(\nu+2-l-t)\,(g_r^2(t)+g_i^2(t))^{1/2}\cos[\theta+\varphi(t)], \quad (16a)$$

where

$$C=2A_2(-2)^{l+1}e^{-\pi K}\Big[\prod_{\lambda=1}^{l}(1+\lambda^2/K^2)/2(1-e^{-2\pi K})\Big]^{1/2},$$

$$\cos\varphi(t)=g_r(t)/(g_r^2+g_i^2)^{1/2},\ \sin\varphi(t)=g_i(t)/[g_r^2(t)+g_i^2(t)]^{1/2},$$

$$g(t)=g_r(t)+ig_i(t)=\tfrac{1}{2}(1+iK/\nu)^{2l+1}\frac{{}_2F_1(\nu+2-l-t,\,-l-iK;\,\nu+3-t-iK;\,(iK-\nu)/(iK+\nu))}{\Gamma(l+1+iK)\Gamma(\nu+3-t-iK)\,(1/\nu+1/iK)^{\nu+3+l-t}}. \quad (16b)$$

${}_2F_1$ is the usual hypergeometric function. The matrix element is similar in structure to that obtained by Burgess and Seaton.[3]

At threshold $(K\to\infty)$,

$$M_{if}=C\sum C_t[M_{\nu+2,l+1/2}(2\nu)\cos(\theta+\pi\nu),$$

$$+(-1)^{l-1-t}\Gamma(2l+2)W_{\nu+2,l+1/2}(2\nu)/\Gamma(\nu+l+3-t)], \quad (17a)$$

where

$$C=A_2e^{-\nu}(\nu)^{\nu+2}/[\sqrt{2}(2l+1)!\cos\pi\nu],$$

$$C_t=b_t\Gamma(\nu+l+3-t)/(\nu)^t. \quad (17b)$$

Here the similarity to the matrix element of Burgess and Seaton[3] is manifest. There the second term in brackets in Eq. (17a) is treated as an additional phase shift in the cosine term. The periodic behavior of the matrix element[3] is a reflection of the periodic behavior of the confluent hypergeometric function.

IV. PARAMETRIZATION OF THE CONTINUUM ORBITALS

Once Z is determined and experimental term values used, Δ is fixed. It is obvious that we cannot closely approximate the charge density of a complex atom with a single parameter Z. The approximation we use for the case of one electron outside a closed shell is to consider the nucleus screened by all those electrons inside the last closed shell, and to locate all the Z-1 electrons in the last closed shell at $r=r_1$. For an electron removed from a partially filled shell, we consider all the closed-shell electrons as completely screening the nucleus, and the remaining electrons in the partially filled shells to be located at $r=r_1$. Admittedly, this is a very crude model, but it should allow us to extend quantum-defect calculations to higher photon energies. Thus, with this model, for helium $Z=2$, for lithium $Z=3$, and for the other alkalis $Z=9$. For the calculations done in the elements from cadmium to xenon, Z increases from 3 for cadmium to 9 for xenon.

As mentioned in Sec. II, there are several values of Δ which can reproduce observed energy eigenvalues in a reasonable way. Table I shows the effective principal quantum numbers for some alkalis[16] and for xenon and krypton.[17] The latter arises from excitation of the outermost filled d shell. The first excited p orbital has $\nu=2.25$. From Fig. 1, we see that with $Z=9$, $\nu\approx2.25$ can be obtained using $\Delta\approx18$, 6, and 3. These values correspond to $r_1\approx1.0$, 2.8, and 5.2 Bohr radii, respectively. For Na, $r_1\approx1.0$ is a reasonable boundary to join

[16] C. Moore, Natl. Bur. Std. Circ. No. 467 (1949).
[17] K. Codling and R. P. Madden, Phys. Rev. Letters **12**, 106 (1964).

the core to a $2/r$ potential,[8] and for the other elements in Table I, $r_1 \approx 2.8$ is the most appropriate of the above three radii. Another criterion, one independent of calculated charge densities, arises from the fact that in the above case, $\Delta \approx 18$ leads to almost hydrogenic d orbitals (i.e., $\nu_{nd} \approx n$), $\Delta \approx 6$ leads to nonhydrogenic d orbitals, but hydrogenic f orbitals ($\nu_{nd} < n$, $\nu_{nf} \approx n$), and $\Delta \approx 3$ leads to nonhydrogenic f orbitals. This reflects the balance of attractive Coulomb potential and repulsive angular-momentum barrier. For sodium the d orbitals are almost hydrogenic, and for the other elements, the f orbitals are almost hydrogenic while the d orbitals are not.

For the calculations reported in Sec. V on helium and the alkalis, the choice of Δ is relevant only through the normalization of the continuum orbital. However, in Sec. VI where we calculate inner-shell photo-ionization cross sections, we include the core and neglect the outer region. There the choice of Δ is relevant to both the normalization and shape of the continuum orbital.

TABLE I. Effective principal quantum numbers for some $l=1$ active electron configurations.

Orbital \ Element	Na	K	Rb	Cs	Xe
$3p$	2.12				
$4p$	3.13	2.23			
$5p$	4.14	3.26	2.29		
$6p$	5.14	4.27	3.33	2.35	2.35
$7p$	6.14	5.28	4.34	3.40	3.40
$8p$	7.14	6.28	5.34	4.41	4.41

V. THE PHOTO-IONIZATION CROSS SECTION OF HELIUM AND THE ALKALIS

Helium. Here $Z=2$, and our continuum orbitals are the exact solutions for the Heisenberg[18] model for the excited states of helium. The $l=1$ effective principal quantum numbers are almost hydrogenic $\nu_{np}=n-0.03$. On a spectrum plot for $Z=2$, $l=1$, these eigenvalues can be reasonably reproduced by $1.70 \leq \Delta \leq 1.90$. For the ground-state orbital, we fitted the Hartree function of Wilson and Lindsay[19] with

$$P_{1s}(r) = 2.88e^{-1.344r}(r)^{0.744}(1. + 0.071/r). \quad (18)$$

The cross section is shown in Fig. 2. Calculation and experiment[20] are in such good agreement that the calculated results for $\Delta = 1.90$ are plotted as discrete points on the experimental curve. Calculation and experiment disagree at shorter wavelengths because of neglect of the inner region.

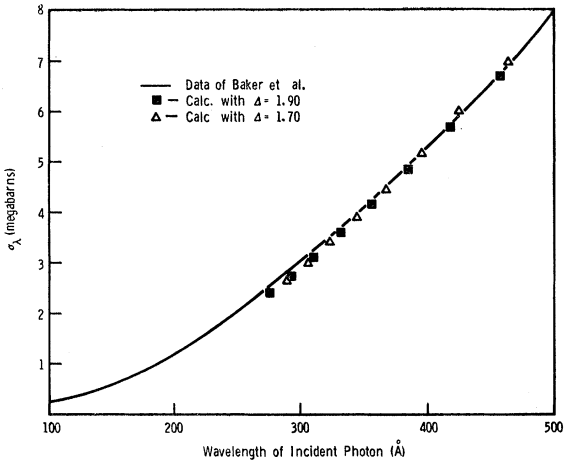

FIG. 2. The photo-ionization cross section of helium.

Lithium. Here, too, the excited p-orbital data is almost hydrogenic ($\nu_{np} \approx n-0.045$). For $Z=3$, $\Delta=3.60$ reproduces these eigenvalues. The $2s$ orbital of Herman and Skillman[8] was fitted with

$$P_{2s}(r) = 0.806e^{-0.629r}(r)^{1.59}(1. - 0.746/r). \quad (19)$$

The cross section is shown in Fig. 3, and compared with a recent measurement of Hudson and Carter.[21] The disparity in the two cross sections is just beyond experimental error. However, the calculated cross section is in agreement with the Hartree-Fock result of Stewart.[22] Hudson and Carter consider Stewart's result in good agreement with their measurement.

Sodium. For sodium the ground-state orbital used was

$$P_{3s}(r) = 0.878(r)^{1.625}e^{-0.615r}(1. - 1.20/r + 0.20/r^2). \quad (20)$$

Table II shows the variation in the $3p$ effective principal quantum number with Δ. The calculated cross section, shown in Fig. 4, is presented for three values of Δ.

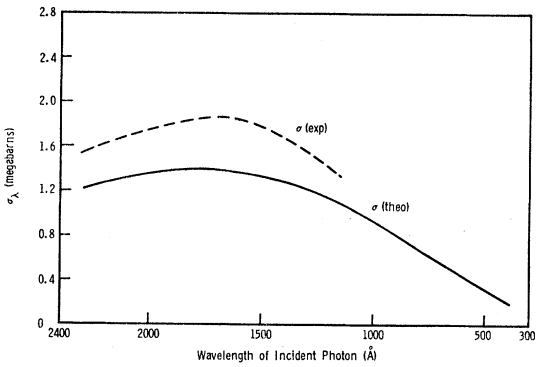

FIG. 3. The photo-ionization cross section of lithium.

[18] W. Heisenberg, Z. Physik **39**, 499 (1927).
[19] W. S. Wilson and R. B. Lindsay, Phys. Rev. **47**, 681 (1935).
[20] D. J. Baker, D. E. Bedo, and D. H. Tomboulian, Phys. Rev. **124**, 1471 (1961).
[21] R. D. Hudson and V. L. Carter, Phys. Rev. **137**, A1648 (1965).
[22] A. Stewart, Proc. Phys. Soc. (London) **67**, 917 (1954).

TABLE II. Effective principal-quantum-number data for Na.

nl	ν_{nl}(exp)	$\nu_{3p}(\Delta=18.6)$	$\nu_{3p}(\Delta=19.1)$	$\nu_{3p}(\Delta=18.0)$
$3p$	2.12	2.120	2.133	2.108

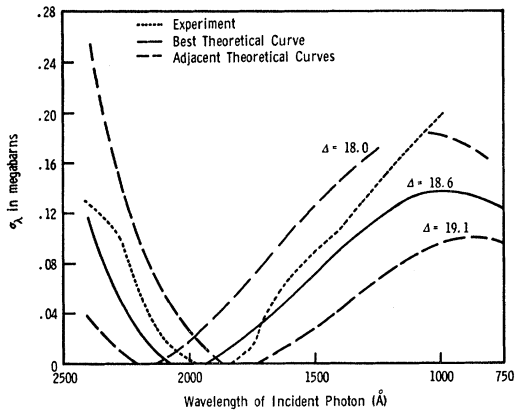

FIG. 4. The photo-ionization cross section of sodium.

TABLE III. Effective principal quantum number data for K.

nl	ν_{nl}(exp)	$\nu_{nl}(\Delta=6.20)$	$\nu_{nl}(\Delta=6.15)$	$\nu_{nl}(\Delta=6.25)$
$4p$	2.23	2.234	2.228	2.239
$5p$	3.26	3.255	3.250	3.261
$6p$	4.27	4.262	4.257	4.267

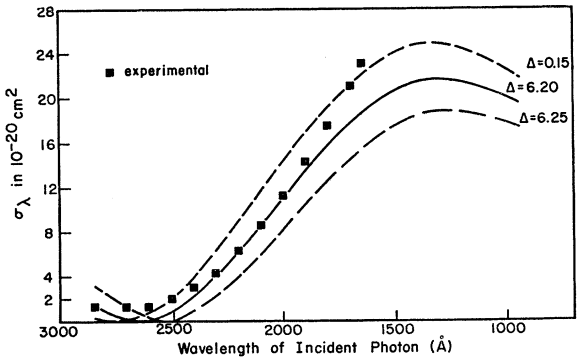

FIG. 5. The photo-ionization cross section of potassium.

TABLE IV. Effective quantum-number data for Rb.

nl	ν_{nl}(expt)	$\nu_{nl}(\Delta=7.0)$	$\nu_{nl}(\Delta=7.1)$
$5p$	2.29	2.287	2.292
$6p$	3.325	3.312	3.318
$7p$	4.34	4.322	4.327

TABLE V. Effective quantum-number data for Cs.

nl	ν_{nl}(exp)	$\nu_{nl}(\Delta=8.30)$	$\nu_{nl}(\Delta=8.10)$
$6p$	2.35	2.370	2.350
$7p$	3.40	3.396	3.378
$8p$	3.41	4.406	4.389

Because of the extensive cancellation in the matrix element the location of the zero in the cross section is a sensitive function of Δ. Comparison with the measurement of Hudson[23] indicates that the calculation which best fits the node does not give the correct rise at higher energies.

The variation of the cross section with Δ is reminescent of calculations by Bates,[24] where the final-state orbital describes an electron in a Hartree potential plus an *ad hoc* polarization potential. Varying the polarizability has much the same effect on the cross section as varying Δ.

Potassium. The ground-state orbital used was[7]

$$P_{4s}(r)=0.773(r)^{1.77}e^{-0.565r}(1.-2.10/r+0.80/r^2). \quad (21)$$

Table III shows the effective principal quantum number data used. Calculated and experimental[25] cross sections are shown in Fig. 5.

Rubidium and Cesium. The ground-state orbitals used were[7]

$$P_{5s}(r)=0.749(r)^{1.805}e^{-0.554r}(1.-2.38/r+1.04/r^2), \quad (22)$$

and

$$P_{6s}(r)=0.701(r)^{1.87}e^{-0.534r}(1.-2.99/r+1.81/r^2). \quad (23)$$

The data used are shown in Tables IV and V, respectively, and calculated and experimental[26] cross sections are shown in Figs. 6 and 7.

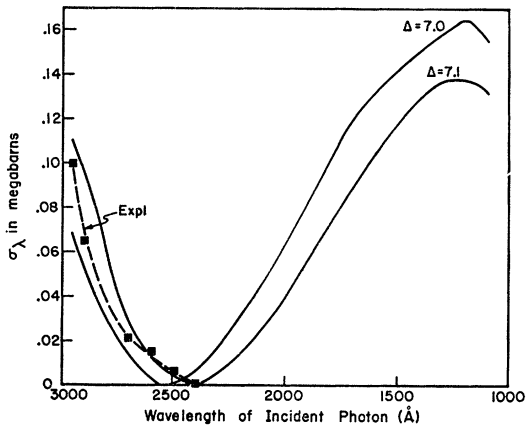

FIG. 6. The photo-ionization cross section of rubidium.

[23] R. D. Hudson, Phys. Rev. **135**, A1212 (1964).
[24] D. R. Bates, Proc. Roy. Soc. (London) **A188**, 350 (1947).
[25] R. W. Ditchburn, J. Tunstead, and J. G. Yates, Proc. Roy. Soc. (London) **A181**, 386 (1943).
[26] R. W. Ditchburn and U. Opik, *Atomic and Molecular Processes*, edited by D. R. Bates (Academic Press Inc., New York 1962).

For all the alkalis except lithium, the ground-state photo-ionization cross section has a zero in the ultraviolet region. This implies that for this region the core cannot be neglected as the small contribution of the core region to the matrix element is relevant to the location of the zero.

VI. INNER-SHELL PHOTO-IONIZATION

Even when we choose an expression such as Eq. (13) as a ground-state orbital, the photoabsorption matrix element requires a numerical integration. However, when either the inner or outer integral in Eq. 12 can be neglected, it is possible to obtain an analytical expression for the matrix element, and, therefore, the cross section. In Sec. III, we treated the first case neglecting the inner integral. When the outer integral can be neglected, the matrix element involves the Laplace transform of the regular confluent hypergeometric function and leads to a hypergeometric function. For a ground-state orbital

$$P_i=A_3e^{-ar}(r)^\nu\sum b_l/r^t, \tag{24a}$$

and for a final-state orbital

$$P_f=B_3M_{\alpha,l+1/2}(2rZ/\alpha), \tag{24b}$$

where A_3 and B_2 are normalization factors, then, for $a>\alpha$, the dipole matrix element is

$$M_{if}=A_3B_3\sum b_l(2Z/\alpha)^{l+1}\frac{\Gamma(l+3-t)\ {}_2F_1(l+1-\alpha,\ l+1+\nu-t;\ 2l+2;\ 2/(1+\alpha a/Z))}{(a+Z/\alpha)^{l+3-t}}. \tag{25}$$

However, since the effective Coulomb central potential for the inner region is not accurate, we restricted the use of Eq. (25) to those transitions in which the angular-momentum quantum numbers are large, e.g., *nd–ef* transitions. For *nf* orbitals the angular-momentum repulsive barrier is much larger than the error in the inner Coulomb potential.

Recently Codling and Madden[17] have used synchrotron radiation to study the photoexcitation of the 4*d* shell in xenon and the 3*d* shell in krypton. They observed transitions of the form $(n\text{-}1d)^{10}(ns)^2(np)^6\rightarrow(n\text{-}1d)^9(ns)^2(np)^6(mp)$, and obtained effective principal quantum-number data for these discrete (auto-ionizing) levels. Since there was no data reported on *d-f* transitions (the *f* levels are probably almost hydrogenic as are the *f* levels in cesium, and, therefore, insensitive to the choice of Δ), we used the *mp* data to choose Δ and fitted the 4*d* xenon orbital of Ref. 8. The calculated and experimental[27] cross sections are shown in Fig. 8.

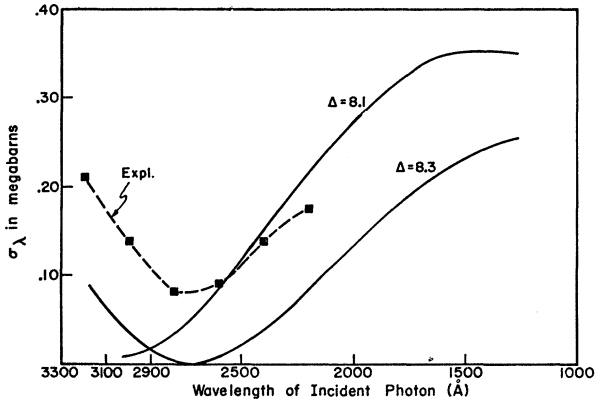

FIG. 7. The photo-ionization cross section of cesium.

The calculated cross section is somewhat sensitive to a variation in the parameter Δ, but with any of these parameters agreement between calculation and experiment must be considered good, considering the approximate inner potential used. There exists a Hartree-Fock calculation[28] of this cross section, but while it is similar in shape to the experimental measurement, it is compressed in energy, indicating that the Hartree-Fock continuum *f* orbital moves too rapidly toward the nucleus with increasing energy.

The success of this calculation on xenon and the availability of 4*d*-shell excitation data on cadmium[16] led us to calculate the 4*d*-shell photo-ionization cross section of the elements from cadmium to xenon. Using $Z-3$, we fitted a Δ to the experimental 4*d–mp* cadmium term values, found a radius r_1 for cadmium, and, using an r_1 determined for xenon, interpolated r_1

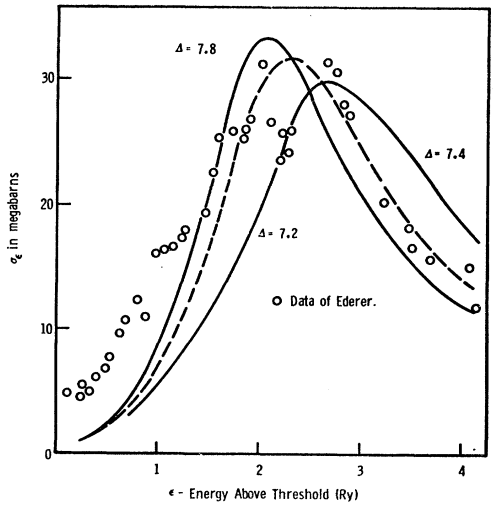

FIG. 8. The photo-ionization cross section of xenon.

[27] D. L. Ederer, Phys. Rev. Letters **13**, 760 (1964).

[28] J. W. Cooper, Phys. Rev. Letters **13**, 762 (1964).

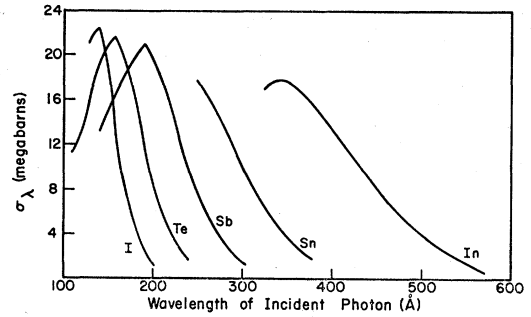

FIG. 9. The photo-ionization cross section of In-Xe.

and Δ for the elements between xenon and cadmium. The cross sections for 4*d* photo-ionization in these elements is shown in Fig. 9. Figure 10 shows the calculated 4*d* photo-ionization cross section, and a measurement[29] of the cross section of a thin film of *Te*. The two curves agree within experimental error. The position of the peak is dependent on the choice of photo-ionization threshold, and the atomic and solid-state thresholds are not the same.[30]

A similar calculation was performed for krypton, using the spectroscopic data of Codling and Madden.[17] The results are shown in Fig. 11. The experimental points were obtained by Lukirskii.[31] Recent measurements made at Cornell[32] indicate that a smooth curve through the points of Lukirskii will fit the experimental 3*d*-shell photo-ionization cross section of krypton. The disagreement between calculation and experiment seems to arise from the compact nature of the krypton 3*d* orbital which would require a more accurate inner potential.

VII. CONCLUSIONS

We have computed one-electron continuum orbitals by developing the exact solutions to a simplified atomic potential. At large distances, the solutions are exactly those one would obtain with the methods of Bates and Damgaard and Burgess and Seaton. However, in our method there is no arbitrary cutoff; all the boundary conditions are taken into account. But the data on experimental term values is used to parametrize the potential, not merely the orbitals. This requires an additional step making calculations more involved than in the asymptotic Coulomb approach.

It was shown that under certain circumstances, exact analytic expressions can be obtained for photo-ionization cross sections. These were used and the agreement between experiment and these calculations were as good as with any other method.

Cross sections for photo-ionization from filled atomic 4*d* shells were performed for the elements indium to xenon. Where experimental data was available for comparison, there was good agreement between calculated and measured cross sections.

This approach is being extended in two ways. Numerical integration of the radial integrals is being done to extend the calculations to systems where neither approximate analytic expression is valid. Secondly, more structure is included in the inner potential to bring it into closer agreement with calculated Hartree charge densities, yet keeping the potential simple enough that it is exactly solvable.

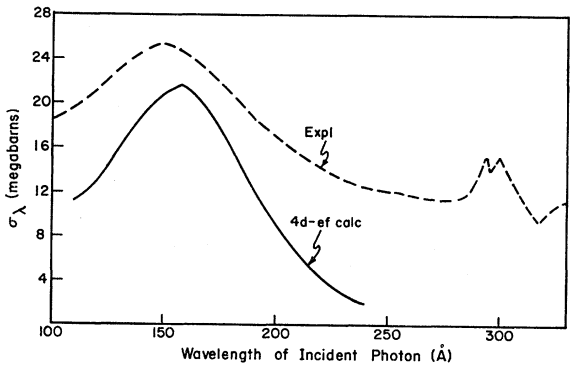

FIG. 10. The photo-ionization cross section of tellurium.

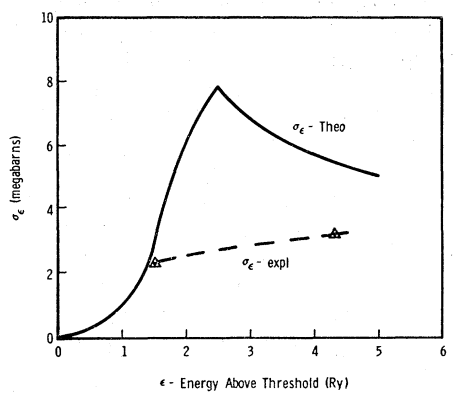

FIG. 11. The photo-ionization cross section of krypton.

ACKNOWLEDGMENTS

The author wishes to express his gratitude to the late Professor D. H. Tomboulian for his support and encouragement of this study; to Professor P. Morrison, Professor D. Holcomb, Dr. H. Schnopper, and Dr. P. Best for their interest and suggestions; to T. Horwitz for his assistance with the programming; and to the Cornell Computing Center for the use of their facilities. He also wishes to thank Mrs. E. Vleck for the typing of the revised manuscript.

APPENDIX A

The regular Whittaker function is well known[9] and easily computed. For the irregular Whittaker function,

[29] R. W. Woodruff and M. P. Givens, Phys. Rev. **97**, 52 (1955).
[30] J. C. Slater, Phys. Rev. **98**, 1039 (1955).
[31] A. P. Lukirskii, I. A. Bryter, and T. M. Zimkina, Opt. i Spektroskopiya **17**, 234 (1964) [English transl.: Opt. Spectry. (USSR) **17**, 438 (1964)].
[32] R. Alexander (private communication).

we used either the asymptotic expansion[14] or the series[11]:

$$\frac{W_{\nu,l+1/2}(2R/\nu)}{\Gamma(l+1+\nu)} = (-1/2R\nu)^l \sin\pi\nu e^{-R/\nu}/\prod_{\lambda=1}^{l}(1-\lambda^2/\nu^2)\pi\nu \left\{\sum_{M=0}^{2l}\frac{\Gamma(\nu+l+1)(2l-M)!}{\Gamma(\nu+l+1-M)M!}\left(\frac{2R}{\nu}\right)^M - \prod_{\lambda=1}^{l}(1-\lambda^2/\nu^2)(2R)^{2l+1}/(2l+1)!\left\{\sum_{j=0}^{\infty}\frac{(-2R/\nu)^j}{j!}\frac{\Gamma(\nu-l)(2l+1)!}{\Gamma(\nu-l-j)(2l+1+j)!}[\ln(2R/\nu)+g(j)]\right\}\right\},$$

where

$$g(0)=\Psi(-\nu+l+1)-\Psi(2l+2)-\Psi(1),$$

$$g(j+1)=g(j)+\frac{1}{l+1+j-\nu}-\frac{1}{2l+2+j}-\frac{1}{1+j},$$

and

$$\Psi(Z)=(d/dZ)\ln\Gamma(Z).$$

APPENDIX B

The general features of Fig. 1 can be obtained from well-known theorems on properties of second-order differential equations. For $\Delta=0$, $r_1\to\infty$ and $\nu_n\to n/Z$, while for $\Delta\to\infty$, $r_1=0$ and $\nu_n\to n$. The contours in Fig. 1 correspond to eigenfunctions with a fixed number of nodes, and as one moves to the right from contour to contour, the number of nodes increases by unity. Further, it can be shown that if $\Delta_n(\nu)$ describes the contour corresponding to eigenfunctions with n nodes, then $d\Delta_n(\nu)/d\nu\geq 0$, so that if r_j is the location of any of these n nodes, then $dr_j/d\nu\geq 0$, i.e., the nodes of the eigenfunction move out from the origin as one moves up the contour.

APPENDIX C

Using the ground-state and continuum orbitals given by Eq. (13) and Eq. (7), respectively, we have

$$M_{if}=AQ(K)\sum_{t=0}b_t[\cos\theta I_1(t)-\sin\theta I_2(t)], \quad \text{(C1a)}$$

where

$$Q(K)=\left\{\prod_{\lambda=1}^{l}\left(1+\frac{\lambda^2}{K^2}\right)\Big/[2(1-e^{-2\pi K})]\right\}^{1/2}, \quad \text{(C1b)}$$

$$I_1(t)=\int_0^\infty (r)^{1+\nu-t}e^{-r/\nu}G_l(r,-1/K^2)\,dr, \quad \text{(C1c)}$$

$$I_2(t)=\int_0^\infty (r)^{1+\nu-t}e^{-r/\nu}(1-e^{-2\pi K})H_l'(r,-1/K^2)\,dr. \quad \text{(C1d)}$$

$I_2(t)$ is finite if $(2+\nu-t-l)>0$.

From the Laplace transforms of the Whittaker functions,[14] we find

$$I_1(t)=B\left(\frac{1}{\nu}+\frac{1}{iK}\right)^{t-\nu-l-3}\left(\frac{iK-\nu}{iK+\nu}\right)^{t-2-\nu+iK}{}_2F_1(l+1+iK,\ l+t-\nu-1;\ 2l+2;\ 2/(1+iK/\nu)), \quad \text{(C2)}$$

$$I_2(t)=iB\left\{\left(\frac{iK-\nu}{iK+\nu}\right)^{t-2-\nu+iK}\left(\frac{1}{\nu}+\frac{1}{iK}\right)^{-(\nu+3+l-t)}{}_2F_1(l+1+iK,\ l+t-\nu-1;\ 2l+2;\ 2/(1+iK/\nu)) - (-1)^{l+1}2e^{-\pi K}\frac{\Gamma(2l+2)}{\Gamma(l+1+iK)}\frac{\Gamma(\nu+2-l-t)}{\Gamma(\nu+3-t-iK)}\left(\frac{1+iK/\nu}{2}\right)^{2l+1}\left(\frac{1}{\nu}+\frac{1}{iK}\right)^{t-\nu-3+l} \times {}_2F_1(\nu+2-l-t,\ -l-iK;\ \nu+3-t-iK;\ (iK-\nu)/(iK+\nu))\right\}, \quad \text{(C3)}$$

where

$$B=2^{l+1}\Gamma(\nu+3+l-t)/\Gamma(2l+2).$$

In Ref. 33, there is quoted a relation between hypergeometric functions from which one can derive

$$\left(\frac{iK-\nu}{iK+\nu}\right)^{t-2-\nu+iK}\frac{{}_2F_1(l+1+iK,\ l+t-\nu-1;\ 2l+2;\ 2/(1+iK/\nu))}{(1/\nu+1/iK)^{\nu+3+l-t}}=(2l+1)!\Gamma(2+\nu-l-t)e^{-\pi K}(-1)^{l+1}(g+g^*),$$

where

$$g(t)=\left(\frac{1+iK/\nu}{2}\right)^{2l+1}\frac{{}_2F_1(\nu+2-l-t,\ -l-iK;\ \nu+3-t-iK;\ (iK-\nu)/(iK+\nu))}{\Gamma(l+1+iK)\Gamma(\nu+3-t-iK)(1/\nu+1/iK)^{\nu+3+l-t}}. \quad \text{(C4)}$$

Then

$$I_1(t)=2(-2)^{l+1}\Gamma(\nu+3+l-t)\Gamma(\nu+2-l-t)e^{-\pi K}\,\mathrm{Re}g(t),$$
$$I_2(t)=2(-2)^{l+1}\Gamma(\nu+3+l-t)\Gamma(\nu+2-l-t)e^{-\pi K}\,\mathrm{Im}g(t). \quad \text{(C5)}$$

[33] Bateman Manuscript Project, *Higher Transcendental Functions*, edited by A. Erdelyi (McGraw-Hill Book Company, Inc., New York, 1953), Vol. I.